

RADIATIVE-DYNAMICAL EQUILIBRIUM STATES FOR JUPITER

L. M. TRAFTON

McDonald Observatory and Astronomy Department, University of Texas at Austin

AND

P. H. STONE

Institute for Space Studies, Goddard Space Flight Center, NASA, New York, N.Y.
 and Department of Meteorology, MIT, Cambridge

Received 1973 June 20; revised 1973 October 1

ABSTRACT

In order to obtain accurate estimates of the radiative heating that drives motions in Jupiter's atmosphere, previous radiative equilibrium calculations are improved by including the NH_3 opacities and updated results for the pressure-induced opacities. These additions increase the radiative lapse rate near the top of the statically unstable region and lead to a fairly constant radiative lapse rate below the tropopause. The radiative-convective equilibrium temperature structure consistent with these changes is calculated, but it differs only slightly from earlier calculations. The radiative equilibrium calculations are used to calculate whether equilibrium states can occur on Jupiter which are similar to the baroclinic instability regimes on the Earth and Mars. The results show that Jupiter's dynamical regime cannot be of this kind, except possibly at very high latitudes, and that its regime must be a basically less stable one than this kind.

Subject headings: atmospheres, planetary — Jupiter

I. INTRODUCTION

In principle the determination of the equilibrium temperature structure of a planetary atmosphere is a highly complex nonlinear problem. The temperature is affected not only by radiative energy fluxes, but also by small- and large-scale dynamical fluxes of sensible and latent heat (Gierasch and Goody 1969). However, recent work (Stone 1972) indicates that Jupiter's atmosphere may be unusually simple in this respect. In particular, even under conditions corresponding to great dynamical stability, the dynamical fluxes are not strong enough to change a superadiabatic radiative state into one with significantly subadiabatic lapse rates. Thus, the traditional approach of taking dynamics into account merely by suppressing superadiabatic lapse rates in a radiative equilibrium calculation should give good results for Jupiter's atmosphere, and one may accept published radiative-convective equilibrium calculations as accurate representations of Jupiter's true radiative-dynamical equilibrium. This situation is in marked contrast to the Earth and Mars where substantial subadiabatic lapse rates are produced by the large-scale motions (cf. the ICAO standard atmosphere for the Earth, and the *Mariner* observations of Mars reported by Rasool and Stewart 1971).

Such radiative-convective equilibrium calculations for Jupiter have been published by Trafton (1967), Hogan, Rasool, and Encrenaz (1969) and Divine (1971). One by-product of these calculations is the radiative equilibrium state that would occur in the adiabatic regions if all motions were suppressed. This hypothetical state is of fundamental interest for studies of dynamics, since the difference between this

state and the adiabatic state is a measure of the strength of the radiative heating which drives the motions. In fact Jupiter's dynamical state is so sensitive to the strength of this heating (Stone 1972) that none of the published calculations are sufficiently accurate to allow one to draw firm conclusions about the dynamics. Trafton's (1967) calculations omit the thermal opacities due to the $10\text{-}\mu$ and rotational bands of NH_3 . These bands make an important addition to the pressure-induced opacities in the adiabatic regions, although they have little impact on the radiative-convective equilibrium temperature structure. Hogan *et al.*'s (1969) calculations are based on a temperature level derived from the $5\text{-}\mu$ observations. As Owen and Westphal (1972) have pointed out, this temperature level is unreliable because of the uncertain geometry of the $5\text{-}\mu$ sources on Jupiter's disk. Divine's (1971) calculations apply to a gray atmosphere, whereas nongray models (Trafton 1967) show that the boundary temperature is significantly less than for the corresponding gray atmosphere having the same effective temperature.

These deficiencies in the published calculations lead us to present in this paper much more accurate radiative equilibrium calculations for Jupiter. Specifically in § II, we will use Trafton's (1967) approach to calculate the radiative equilibrium structure, but with recent results for the $\text{H}_2\text{-He}$ opacity (Trafton 1973) and for the NH_3 opacity (Gille and Lee 1969) included. In § III we will calculate the radiative-convective equilibrium structure consistent with the results of § II. Finally in § IV we will use these results to calculate whether an equilibrium state corresponding to a baroclinic instability regime can exist on Jupiter.

TABLE 1
 RADIATIVE-EQUILIBRIUM MODEL FOR JUPITER

τ_s	$\langle \tau \rangle$	T (° K)	$\log_{10} P$ (dynes cm ⁻²)	[H ₂] (km amagats)	ρ (g cm ⁻³)	h (km)	∇_a
0.000	0.0	105.6	3.843	0.26	1.694(-6)	0.	0.352
0.003	0.001	105.6	4.231	0.63	4.263(-6)	14.4	0.355
0.008	0.002	106.1	4.444	1.03	6.927(-6)	22.3	0.354
0.020	0.005	106.8	4.643	1.63	1.088(-5)	29.7	0.354
0.035	0.009	107.5	4.764	2.16	1.430(-5)	34.2	0.353
0.080	0.021	109.4	4.945	3.27	2.129(-5)	41.0	0.352
0.15	0.041	111.8	5.083	4.49	2.862(-5)	46.3	0.350
0.30	0.084	115.7	5.270	6.91	4.215(-5)	53.1	0.347
0.50	0.146	119.9	5.349	8.30	4.933(-5)	57.0	0.345
0.70	0.212	123.3	5.425	9.87	5.707(-5)	60.2	0.342
1.00	0.321	127.6	5.505	11.9	6.636(-5)	63.7	0.339
1.40	0.486	132.4	5.582	14.2	7.624(-5)	67.2	0.336
1.80	0.676	136.9	5.639	16.2	8.422(-5)	69.9	0.332
2.00	0.780	139.0	5.664	17.1	8.768(-5)	71.1	0.330
2.50	1.07	144.8	5.715	19.3	9.484(-5)	73.6	0.322
3.0	1.38	150.8	5.758	21.3	1.004(-4)	75.8	0.328
3.5	1.68	156.2	5.794	23.1	1.054(-4)	77.7	0.326
4.0	2.00	160.9	5.826	24.8	1.100(-4)	79.5	0.324
5.0	2.62	169.7	5.879	28.1	1.180(-4)	82.6	0.320
6.0	3.24	176.5	5.923	31.1	1.257(-4)	85.2	0.318
8.0	4.48	189.1	5.995	36.7	1.382(-4)	89.8	0.314
10.0	5.69	199.5	6.051	41.7	1.491(-4)	93.6	0.311
14.0	8.09	216.6	6.137	50.9	1.676(-4)	99.8	0.307
18.0	10.5	230.3	6.203	59.3	1.833(-4)	104.9	0.304
22.0	12.8	241.9	6.256	67.0	1.972(-4)	109.3	0.302
26.0	15.1	252.1	6.301	74.2	2.097(-4)	113.1	0.300
30.0	17.3	261.1	6.339	81.0	2.210(-4)	116.5	0.299

NOTE.— $T_e = 135^\circ \text{K}$; $\text{He}/\text{H}_2 = 0.1$; Max. $\text{NH}_3/\text{H}_2 = 1.7 \times 10^{-4}$; $\text{CH}_4/\text{H}_2 = 3.0 \times 10^{-3}$; $g = 2500 \text{ cm s}^{-2}$; $\tau_s \equiv$ optical depth at 520 cm^{-1} ; $\langle \tau \rangle \equiv$ Rosseland mean optical depth; $\nabla_a \equiv$ adiabatic gradient.

II. RADIATIVE EQUILIBRIUM

Because of the preceding considerations, we employ essentially the method outlined by Trafton (1967) to compute radiative models of Jupiter's atmosphere. The major differences are that we ignore convection here, include the thermal opacities of NH_3 and use updated pressure-induced absorption coefficients. The validity of this method is restricted to the region of Jupiter's atmosphere where the thermal opacities are significant. This means that our models do not apply in the region of the temperature inversion. This region can exist only in the uppermost part of Jupiter's atmosphere where the pressure-induced opacity becomes negligibly small. Only in this circumstance can a temperature inversion result from the sunlight absorbed by the near-infrared CH_4 bands since the mechanism for the radiation of the thermal energy from these levels is effectively removed. For this reason, these two regions decouple and we refer to the part of the atmosphere underlying the inversion layer as the "thermal regime." Our models apply only to this regime.

Specifically, the following improvements have been made in the pressure induced opacities: First, we brought the line profile into agreement with the shapes found by MacTaggart and Hunt (1969). These have a power-law tail matched to a modified Lorentz core. The same line shape was assumed for the He-H_2 enhancement. Second, we revised the absorption

coefficient for the He-H_2 enhancement, as described by Trafton (1973), to include a more realistic value of the overlap parameter in the induced dipole moment. Previously, the value for $\text{H}_2\text{-H}_2$ collisions was assumed for the He-H_2 enhancement. Third, we included both the rotational and the $10\text{-}\mu$ NH_3 opacities assuming saturation of the NH_3 vapor in Jupiter's atmosphere down to a level where the NH_3/H_2 mixing ratio is given by the solar abundance ratio, 1.7×10^{-4} (Lambert 1968). The values of Gille and Lee (1969) were employed in a manner which accounts to first order for the discrete line structure of these bands (cf. Wildey and Trafton 1971). We have not included the thermal opacity of the $7.5\text{-}\mu$ CH_4 band but this omission is compensated to some degree by our setting the flux to zero for frequencies greater than 1500 cm^{-1} .

We have taken no account of the absorption of sunlight by molecular bands at various depths within the atmosphere. Jupiter's spectrum suggests that 10 percent of the sunlight is absorbed above the clouds shortward of 2.5μ (Trafton and Münch 1969). However, the flux from Jupiter's internal heat source is nearly 2 times the solar insolation so that the net flux should be constant with depth to about 3 percent over the visible region of the atmosphere. We neglect this small variation and calculate constant flux models with effective temperature near the value $T_e = 134^\circ \text{K}$ obtained by Aumann, Gillespie, and Low (1969). Also, we have taken no account of scattering by cloud

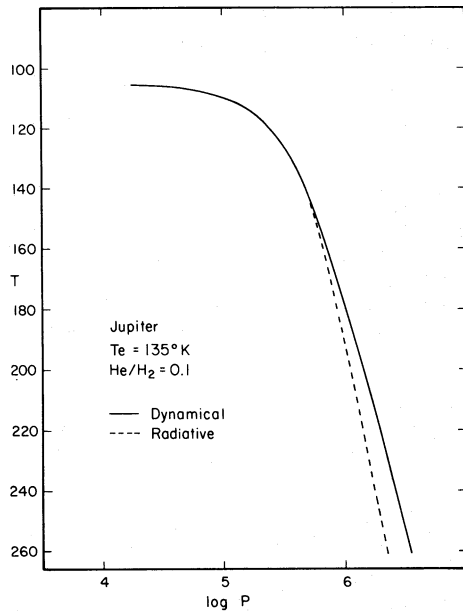


FIG. 1.—Temperature-pressure relationship for Jupiter showing the effect of the dynamics.

particles. The presence of scattering particles in the regions with dynamics would increase the radiative temperature gradient, but would not affect the adiabatic structure calculated in § III below. The scattering would also increase the radiative heating, but such an increase would only reinforce the conclusions we will reach in § IV about the dynamical regime. Table 1 lists the structure for radiative equilibrium and a He/H₂ ratio equal to 0.1, a value also near the solar ratio. Figure 1 presents the $P(T)$ dependence for comparison with the earlier calculations of Trafton (1967). Note that no temperature inversion results strictly from the nongray character of the opacity, such as that discussed by Goody (1964) for the case of a gas mixture in which each gas has a different vertical distribution of opacity.

The quantity of specific interest for dynamical studies in these models is the radiative gradient $\nabla_r \equiv d \ln T / d \ln P$ as a function of temperature. Because of the iterative method of solution to obtain flux constancy, the temperature and pressure points of the model are uncertain by amounts which show little correlation from point to point. This causes the radiative gradient to be noisy since it was obtained by numerical differentiation. As Goodman (1969) has shown, the radiative gradient can be expressed in terms of Schwarzschild's approximation (1958) for the radiative flux in the optically deep layers of the atmosphere and this can be used to verify the values of ∇_r derived from the models. This approximation yields

$$\nabla_r = \frac{3}{16} \frac{kT}{\mu m_{\text{H}} g} \left(\frac{T_e}{T} \right)^4 \langle K \rangle, \quad (1)$$

where $\langle K \rangle$ is the Rosseland mean absorption coeffi-

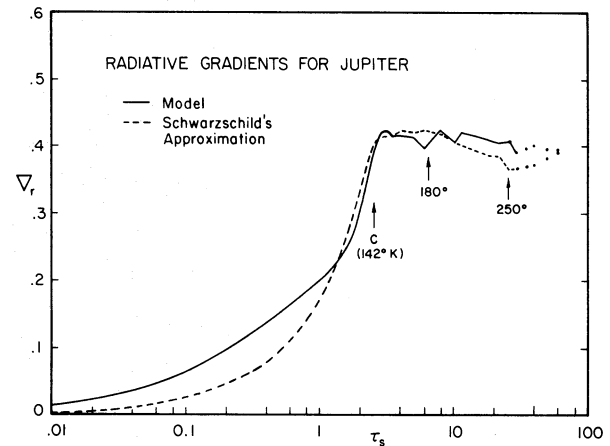


FIG. 2.—Jupiter's radiative gradient. The dashed line is from Goodman's expression (eq. [1]) using Schwarzschild's approximation for the radiative flux. The agreement is good in the deeper layers. The dots indicate uncertainty in ∇_r caused by incomplete convergence to flux constancy of the deepest layers. The arrows denote temperatures ($^{\circ}$ K) corresponding to τ_s , the optical depth at 520 cm^{-1} . The symbol C denotes where the radiative zone ends.

cient per unit length, g is the surface gravity, m_{H} is the mass of the hydrogen atom, μ is the mean molecular weight, k is Boltzmann's constant and T is the local temperature. Figures 2 and 3 compare the radiative gradients obtained from several models in radiative equilibrium with those obtained from Goodman's approximate expression. These show the extent to which the numerical derivative is reliable. Thus, the numerical value of the radiative gradient at the 180 $^{\circ}$ K level, corresponding roughly to the deepest dynamical phenomena which are visible, should be accurate to ± 0.015 . For the model of table 1, we obtain a radiative gradient of 0.41 at this level (cf. fig. 2). This value is not sensitive to the NH₃/H₂ mixing ratio in a wide

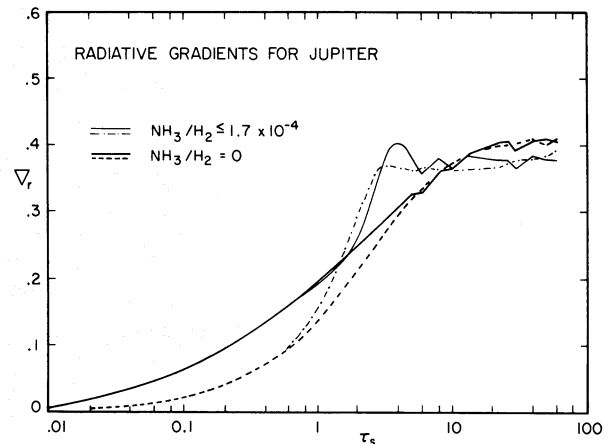


FIG. 3.—The effect of the rotational NH₃ band on Jupiter's radiative gradient. The broken lines are derived from the approximation given by equation (1). The mixing ratio NH₃/H₂ is 1.7×10^{-4} in the layers where NH₃ is not saturated. The discontinuities in slope are artifacts of the numerical truncation error. The 10- μ NH₃ opacity is omitted in this comparison.

neighborhood of solar values, nor is it particularly sensitive to the He/H₂ ratio for values in such a neighborhood.

The rapid rise and following plateau in the radiative gradient for this model also occurs for the approximate expression, equation (1). For a pressure induced opacity, the radiative gradient varies as N^2/T^3 where N is the number density. In the optically shallow region of the atmosphere, T is nearly constant, so ∇_r increases as N^2 . Deeper in the atmosphere, the opacity of the saturated NH₃ causes an even more rapid variation with depth. After the thermal opacity becomes effective, and after the termination of NH₃ saturation, the resulting increase of T offsets the increase in N^2 to bring ∇_r to at least a temporary plateau. The sudden termination of NH₃ saturation is responsible for the sharp edge of this plateau, as is shown in figure 3.

The effect on the radiative gradient of combining the opacity of the NH₃ rotational band with the pressure-induced opacity is also illustrated in figure 3. The effect of further adding the 10- μ band merely raises the plateau from 0.36 to 0.41 at the 180° K level, as comparison with figure 2 shows. Note that for the shallower layers, the effect of adding the NH₃ opacity is to raise ∇_r , while for the deeper layers it reduces the value of ∇_r . This behavior can be understood in terms of the dependence of equation (1) on the temperature and the Rosseland mean opacity. After the addition of NH₃, there will be two opposing effects operating on the radiative gradient. On the one hand, the increase in $\langle K \rangle$ will tend to increase ∇_r . On the other hand, the increase in backwarming from the additional opacity will increase the temperature and this will tend to decrease ∇_r . Even if a level at constant temperature is considered (instead of constant pressure), adding the NH₃ opacity will lower the pressure of that level owing to the increased backwarming. The lower pressure, in turn, reduces the opacity. This competes with the increase in opacity caused by the addition of NH₃. In the cooler, optically shallow region, the increase in $\langle K \rangle$ dominates because the backwarming is not yet strong and because the overlap of the rotational NH₃ band with the normalized Planck function is greater at lower temperatures. In the deeper regions, the overlap is less owing to the higher temperatures caused by the new efficient backwarming. Here, the increase in temperature dominates the increase in $\langle K \rangle$. Note that the addition of the 10- μ NH₃ band favors an increase in ∇_r because this band overlaps the Planck function more efficiently in the deeper layers.

III. EFFECT OF DYNAMICS

As discussed in the introduction, we may include the effect of dynamics on the temperature structure merely by suppressing superadiabatic lapse rates—i.e., in the regions where the radiative temperature lapse rate exceeds the moist adiabatic lapse rate, we will replace the former by the latter. This method is not rigorous, since the radiative energy flux emerging from the

TABLE 2
EFFECT OF He/H₂ AND T_e ON DYNAMICAL PARAMETERS*

T_e	He/H ₂	τ_c	T_c	log P_c	∇_r
120.....	0	3.5	130	5.71	0.41†
120.....	1	3.3	137	6.20	0.37
140.....	0	2.0	140	5.59	0.35
140.....	1	1.8	142	5.90	0.34

* Quantities subscripted c denote values at the top of the convective zone.

† These values apply to one scale height below the top of the convective zone. We have neglected the 10- μ NH₃ band in this comparison.

adiabatic regions below the tropopause will now be less than the total flux necessary to have radiative equilibrium at and above the tropopause. In reality, the tropopause will be at a higher level than the one where the radiative lapse rate first equals the adiabatic lapse rate. However, taking the latter level to be the tropopause will only introduce a small error in the case of Jupiter, since the radiative lapse rate below this level remains close to the adiabatic lapse rate (see fig. 1). A graphical estimate shows that the real tropopause would be at a temperature level about 5° K colder than the level where the radiative lapse rate first equals the adiabatic lapse rate, and that the change in the temperature at a given pressure below the tropopause resulting from this displacement of the tropopause is only about 1.5° K.

In order to verify that our conclusions concerning the role that dynamics plays is not affected by the uncertainties in the He/H₂ ratio or effective temperature, we have calculated model atmospheres for several extreme combinations of these parameters, neglecting the 10- μ NH₃ band. The temperature, pressure, and optical depth at the standard wavelength corresponding to the top of the convective zone is presented for each model in table 2 along with the radiative gradient one scale height below the top of the convective zone. These quantities govern the dynamical regime discussed in the next section. The variation indicated in table 2 does not alter our conclusions on the role that dynamics plays.

The altered structure resulting from the inclusion of dynamics is listed in table 3 and illustrated for $P(T)$ in figure 1. The wet adiabat, in what is traditionally referred to as the "convective region," now approximates the effect of all dynamics, whether large or small scale, and the "radiative zone" represents the boundary region of the atmosphere, which is controlled by the escape of thermal radiation to space. We note that the more accurate thermal opacities used here do not change the radiative-convective equilibrium structure very much (cf. Trafton 1967).

IV. DYNAMICAL REGIME

A variety of possible dynamical regimes for Jupiter have been discussed in the literature (see Stone 1973 for a review). Since radiative heating is the primary

TABLE 3
JOVIAN STRUCTURE CORRECTED FOR DYNAMICS*

τ_s	T (° K)	$\log_{10} P$ (dynes cm ⁻²)	[H ₂] (km amagats)	ρ (g cm ⁻³)	h (km)
2.00†	139.0	5.664	17.1	8.768(-5)	71.1
2.61	144.8	5.717	19.3	9.521(-5)	73.8
3.37	150.9	5.773	22.0	1.039(-4)	76.7
4.16	156.2	5.819	24.5	1.116(-4)	79.2
4.95	160.9	5.859	26.8	1.188(-4)	81.5
6.88	169.7	5.930	31.6	1.362(-4)	85.7
8.65	176.5	5.984	35.8	1.444(-4)	89.0
13.3	189.1	6.079	44.5	1.677(-4)	95.2
18.2	199.5	6.153	52.8	1.885(-4)	100.4
30.1	216.6	6.269	69.0	2.268(-4)	109.1
42.6	230.3	6.356	84.3	2.606(-4)	116.1
55.8	241.9	6.427	99.2	2.922(-4)	122.1
69.7	252.1	6.486	113.7	3.212(-4)	127.3
84.3	261.1	6.537	127.8	3.487(-4)	131.9

* The variables have the same definitions as given in table 1.

† For the shallower layers, the structure of table 1 applies.

drive for the motions, any complete theory for Jupiter's dynamical regime must include this drive and show that the balance between the radiative heating and the dynamical cooling is consistent with the assumed dynamical regime. The only regime for which such a balance has been calculated is the baroclinic instability regime (Stone 1972). Since the results are sensitive to the amount of radiative heating, we will use the results of § II to calculate more accurately than previously whether such a regime can exist on Jupiter. The data of § II should also be of use in calculating whether other regimes can exist once the equations describing the appropriate equilibria are developed.

The most important parameter governing the dynamical regime is the Richardson number,

$$Ri = \frac{g\partial\theta/\partial z}{T(\partial u/\partial z)^2} \quad (2)$$

Here z is the vertical position, θ the potential temperature, and u the zonal velocity. Different kinds of instability can dominate the motions, depending on the mean value of Ri (Stone 1966). Large negative values imply the most unstable possible regime, one dominated by vigorous small-scale convection of the kind associated with simple static stability. Large positive values imply the most stable possible regime. If $Ri > 1$ then the dominant kind of instability is geostrophic baroclinic instability (Stone 1966) the kind that occurs on the Earth and apparently also on Mars (Leovy and Mintz 1969; Stone 1972). Under such stable conditions barotropic instability (Ingersoll and Cuzzi 1969) may also occur, but it does not transport heat and therefore does not enter the energy-balance equation. Similarly, the radiative instability described by Gierasch (1973) is unlikely to play a significant role in the energy balance under such stable conditions, since its growth rates are much smaller than those for baroclinic instability. Therefore, the most stable regime likely to occur on Jupiter is one

like that on the Earth and Mars, in which the radiative heating is primarily balanced by dynamical fluxes due to baroclinic instabilities. The equilibria corresponding to such a regime should at least give an upper bound to the actual values of Ri and $\partial\theta/\partial z$ on Jupiter. In principle such an equilibrium could extend to much lower latitudes on Jupiter than on the Earth or Mars, since the scale of baroclinic instabilities on Jupiter would be much smaller relative to the planet's size. Gierasch, Goody, and Stone (1970) estimated an upper bound for this scale of about 2000 km, which implies that a baroclinic instability regime could occur everywhere on Jupiter except within a few degrees of the equator.

In the previous calculations of this kind of equilibrium (Stone 1972) the radiative heating was approximated by a linearization about the radiative equilibrium state, of the kind introduced by Spiegel (1957) and generalized by Goody (1964) for a nongray gas. This approximation allows the radiative heating to be calculated simply from a knowledge of the radiative equilibrium state and the radiative relaxation time. The approximation is a good one for Jupiter since the temperature in the radiative and radiative-dynamical equilibrium states are close (see fig. 1). In the top scale height of the adiabatic region the temperature differences and therefore the error are at most 10 percent. The calculations for the dynamical cooling neglected deep atmosphere effects and condensation. These approximations also appear to be good ones. McIntyre (1972) has shown that the fluxes due to baroclinic instabilities are qualitatively the same for a baroclinic layer in a deep atmosphere as for a baroclinic layer above a rigid boundary. The ammonia saturation level for the model given in tables 1 and 3 is 146° K—i.e., condensation only occurs in the top 3 km of the adiabatic region. Consequently the overall structure of the adiabatic region is not affected by condensation. Even in the condensing layer the effect on the temperatures is negligible, since the dry and moist adiabatic lapse rates differ by less than 2 percent. The

ammonia concentration would have to be an order of magnitude larger in order to affect our estimates below. Also the layers of interest here are well above the levels where other significant condensates occur (Lewis 1969).

The results of the earlier calculations showed that, even allowing for uncertainty in the amount of radiative heating, the static stability must be very small—i.e., $\partial\theta/\partial z \leq 0$ ($10^{-3} \text{ }^\circ \text{ K km}^{-1}$). It is this result which allows one to accept radiative-convective equilibrium calculations as a good approximation to the true radiative-dynamical equilibrium structure. However, the uncertainty in the heating prevented meaningful bounds from being placed on the Richardson number. Using the results of § II, we can now find such bounds. For Jupiter the mean equilibrium value of Ri corresponding to a balance between radiative heating and dynamical cooling by baroclinic instabilities is given by (Stone 1972, § IIIc)

$$\text{Ri} \simeq \frac{kg\tau_R^2(\partial T_r/\partial\Phi)^4}{1.93f^2T^2\mu^2m_H^2R^4(\nabla_r - \nabla_a)^2} - 1. \quad (3)$$

Here τ_R is the radiative relaxation time, Φ is the latitude, T is the temperature of the radiative equilibrium state, f is the coriolis parameter,

$$f = 2\Omega \sin \Phi, \quad (4)$$

Ω is the angular rate of rotation, R is the planetary radius, and ∇_a is the adiabatic value of $\partial \ln T/\partial \ln P$. We will model the Φ dependence of T_r by assuming a $\cos \Phi$ distribution of solar insolation and a uniform distribution of heating from the interior, so that

$$T_r(P, \Phi) = \bar{T}_r(P) \left[\frac{(4/\pi) \cos \Phi + q}{1 + q} \right]^{1/4}, \quad (5)$$

where $\bar{T}_r(P)$ is the global mean vertical temperature distribution in radiative equilibrium, and q is the ratio of the total flux of heat from the interior to the total flux from the Sun.

The gradients of T_r which enter equation (3) are mean values for the regions where solar radiation is absorbed. The levels where this occurs are not well determined, but probably fall between the tropopause and one scale height below the tropopause. In this region the temperature lies in the approximate range $140^\circ\text{--}200^\circ \text{ K}$ (see table 3). Because of the uncertainty in the location of these layers, we will calculate Ri by evaluating the right-hand side of equation (3) for various levels in the range $140^\circ \text{ K} < T_r < 200^\circ \text{ K}$. In addition the right-hand side is formally a function of latitude. Since the characteristic scale of baroclinic instabilities on Jupiter would be much less than the planetary radius (Gierasch *et al.* 1970) variations of Ri with latitude would represent actual changes in the equilibrium value with latitude. Consequently we shall also calculate Ri as a function of latitude. For the fixed parameters we will adopt the values $g = 2500 \text{ cm s}^{-1}$; $\Omega = 1.76 \times 10^{-4} \text{ s}^{-1}$, $R = 71,000 \text{ km}$, $q = 1.7$ (Aumann *et al.* 1969) and $\mu = 2.2$. The radiative relaxation times for different levels were taken from

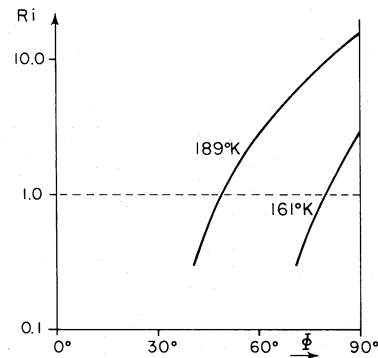


FIG. 4.—Equilibrium value of Richardson number versus latitude.

Gierasch and Goody's (1969) data. In determining the appropriate time scale the density values given in table 3 were used, and the dominant wavenumber for the motions was assumed to be π/H where H is the local scale height. $T_r(P)$ and ∇_a were taken from table 1.

Figure 4 shows how the Richardson number would vary with latitude if the 161° or 189° K levels are chosen as typical of the layers where solar radiation is absorbed. The most important question is whether $\text{Ri} > 1$ or $\text{Ri} < 1$. Only in the former case does baroclinic instability dominate so that equation (3) is applicable (Stone 1972). If $\text{Ri} < 1$ other instabilities dominate and one can only conclude that a baroclinic instability regime cannot exist. In figure 5, the critical latitude at which $\text{Ri} = 1$ is plotted as a function of level. In spite of the uncertainty in the location of the level typical of the layers where solar radiation is absorbed, it is possible to conclude that for these layers as a whole, at sufficiently low latitudes Jupiter's dynamical regime must differ fundamentally from those on Earth and Mars. A reasonable value for the critical latitude where $R = 1$, is $\Phi = 70^\circ$. The dynamical regime in higher latitudes is still open to question. Even if $\text{Ri} > 1$ baroclinic instabilities could be eliminated by deep atmosphere effects not present on the Earth or Mars (McIntyre 1972). The conclusion about the low-latitude regime could be changed if the internal heat source is found to be nonuniform in latitude or if the ammonia mixing ratio is much larger than we assumed.

The nature of the less stable low-latitude regime has yet to be determined. Three suggestions have been

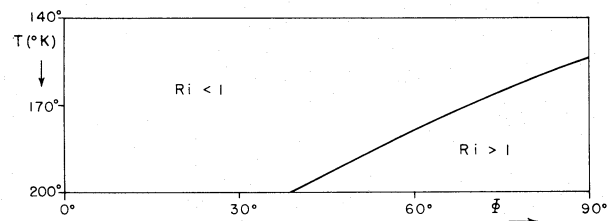


FIG. 5.—Temperature level at which $\text{Ri} = 1$, versus latitude.

made which are consistent with the criterion $Ri < 1$ and which can lead to banded structures like those observed in Jupiter's low latitudes. These are: (1) an inertial instability regime (Stone 1971); (2) a free convection regime (Williams and Robinson 1973) and (3) a coupled radiation-condensation instability regime (Gierasch 1973). The second of these, the free-convection regime, would occur for large negative values of Ri but it seems to be an implausible suggestion for Jupiter since it can only account for the observed banded structure if the internal heat source is orders of magnitude larger than it is currently believed to be. The other two regimes can occur for small positive values of Ri and the growth rates of the corresponding types of instability are competitive if

$\partial\theta/\partial z$ is sufficiently small. In fact, both the inertial instability and the radiation-condensation instability generate very similar banded structures, and it is possible that the two kinds of instability act simultaneously and reinforce each other. One other kind of regime that is consistent with the criterion $Ri < 1$ is a forced convection regime, i.e., one with small negative values of Ri . In such a regime small-scale convection would be the dominant mode, but it would be significantly modified by the presence of a zonal thermal wind. No studies of this regime have been published.

This research was supported in part by NASA grant NGR-012-152.

REFERENCES

- Aumann, H. H., Gillespie, C. M., and Low, F. J. 1969, *Ap. J. (Letters)*, **159**, L69.
 Divine, T. N. 1971, *The Planet Jupiter (1970)*, NASA SP-8069.
 Gierasch, P. J. 1973, *Icarus*, **19**, 482.
 Gierasch, P. J., and Goody, R. M. 1969, *J. Atm. Sci.*, **26**, 979.
 Gierasch, P. J., Goody, R. M., and Stone, P. H. 1970, *Geophys. Fluid Dyn.*, **1**, 1.
 Gille, J. C., and Lee, T. H. 1969, *J. Atm. Sci.*, **26**, 932.
 Goodman, G. C. 1969, unpublished Ph.D. thesis, University of Illinois.
 Goody, R. M. 1964, *Atmospheric Radiation* (London: Oxford University Press), pp. 339-341.
 Hogan, J. S., Rasool, S. I., and Encrenaz, Th. 1969, *J. Atm. Sci.*, **26**, 898.
 Ingersoll, A. P., and Cuzzi, J. N. 1969, *J. Atm. Sci.*, **26**, 981.
 Lambert, D. L. 1968, *M.N.R.A.S.*, **138**, 143.
 Leovy, C., and Mintz, Y. 1969, *J. Atm. Sci.*, **26**, 1167.
 Lewis, J. S. 1969, *Icarus*, **10**, 365.
 MacTaggart, J. W., and Hunt, J. L. 1969, *Canadian J. Phys.*, **47**, 65.
 McIntyre, M. E. 1972, *Quart. J. Roy. Meteorol. Soc.*, **98**, 165.
 Owen, T., and Westphal, J. A. 1972, *Icarus*, **16**, 392.
 Rasool, S. I., and Stewart, R. W. 1971, *J. Atm. Sci.*, **28**, 869.
 Schwarzschild, M. 1958, *Structure and Evolution of the Stars*, (Princeton, New Jersey: Princeton University Press).
 Spiegel, E. A. 1957, *Ap. J.*, **126**, 202.
 Stone, P. H. 1966, *J. Atm. Sci.*, **23**, 390.
 ———. 1971, *Geophys. Fluid Dyn.*, **2**, 147.
 ———. 1972, *J. Atm. Sci.*, **29**, 405.
 ———. 1973, *Space Sci. Rev.*, **14**, 444.
 Trafton, L. M., 1967, *Ap. J.*, **147**, 765.
 ———. 1973, *ibid.*, **179**, 971.
 Trafton, L. M., and Münch, G. 1969, *J. Atm. Sci.*, **26**, 813.
 Wildey, R. L., and Trafton, L. M. 1971, *Ap. J. Suppl.*, **23**, 1.
 Williams, G. P., and Robinson, J. B., 1973, *J. Atm. Sci.*, **30**, 684.

